

Bayesian CycleGAN via Marginalizing Latent Sampling

Haoran You¹ Yu Cheng^{2,†} Tianheng Cheng^{1,†} ChunLiang Li^{3,†} Pan Zhou¹

¹Huazhong University of Science and Technology ²Microsoft AI and Research

³Machine Learning department, Carnegie Mellon University

Abstract

Recent techniques built on Generative Adversarial Networks (GANs) like CycleGAN are able to learn mappings between domains from unpaired datasets through min-max optimization games between generators and discriminators. However, it remains challenging to stabilize training process and diversify generated results. To address these problems, we present a Bayesian extension of cyclic model and an integrated cyclic framework for inter-domain mappings. The proposed method stimulated by Bayesian GAN explores the full posteriors of Bayesian cyclic model (with latent sampling) and optimizes the model with maximum a posteriori (MAP) estimation. Hence, we name it Bayesian CycleGAN. We perform the proposed Bayesian CycleGAN on multiple benchmark datasets, including Cityscapes, Maps, and Monet2photo. The quantitative and qualitative evaluations demonstrate the proposed method can achieve more stable training, superior performance and diversified images generating.

1. Introduction

The problem of learning mappings between different domains has recently received increasing attention, especially for image-to-image translation like semantic segmentation and style transfer. Within unsupervised setting, this task becomes challenging but also important as supervision may be scarce or otherwise difficult to obtain in most scenarios.

To solve this issue, several solutions have been proposed, including methods relied on cycle consistency constraints such as CycleGAN [27, 13, 25, 21], while others relied on weight sharing constraints [17, 16, 10]. Given the unpaired dataset, the cyclic model was proposed to learn image-to-image translation from a source domain X to a target domain Y . Built upon Generative Adversarial Networks [6], the model is able to learn a good generator which produces images in one domain given images from the other by satis-

fy marginal matching (GAN loss for each mapping) and cycle-consistency constraints. The existing cyclic model can achieve balance between generators and discriminators with elaborate setting of hyper-parameters and other tricks like buffering generated images, avoiding the untimely success of discriminators. Otherwise it would be difficult for the cyclic model to remain stable. Moreover, the model cannot realize diversified generating with a stochastic variable z due to the fundamental flaw of original cyclic model: the cycle-consistency encourages the mappings to ignore the stochastic latent variable [1].

To improve the stability and performance of the CycleGAN model, in this paper, we propose its Bayesian extension with regularized priors called Bayesian CycleGAN, optimizing with maximum a posteriori (MAP) estimation. By exploring the full posteriors with latent sampling over parameters, Bayesian cyclic model enhances the generators training to resist crazy learning discriminators. Therefore, Bayesian CycleGAN alleviates the risk of *model collapse*, boosting realistic color generating and multimodal distribution learning. Our work is inspired by the recent success of the Bayesian GAN [22], which aims to model the true data distribution more accurately by fully representing the posterior distribution over the parameters of both the generator and discriminator. However, there is a non-negligible issue for Bayesian GAN to be applied to cyclic learning directly since the Bayesian GAN forms posteriors by sampling generators $\theta_g \sim p(\theta_g)$, which cannot transfer to cyclic framework. If we sampled the two generators of cyclic framework simultaneously, the memory consumption would increase sharply due to the nature of cyclic framework, and the reconstructed images would be skumble-scumble so that the update of parameters could not match the cycle-consistency loss. Instead of sampling among networks, we use variant-concatenate inputs that combine the source images and sampled latent variables.

As mentioned above, the diversified generation issue is caused by the reason that the cycle-consistency encourages the mappings to ignore z . Thinking outside of the box, we can divide the latent space and use only one part of that to fit in training process. Therefore, it is feasible for us to diver-

[†] denotes equal contribution; We have made code and tutorial available at <https://github.com/ranery/Bayesian-CycleGAN>

sify the generated images in inference process by replacing the restricted one with other latent variables. Specifically, we use a VAE-like encoder network to generate the latent variable *statistic feature map (SFM)* which remains much the same for each domain, substituting latent variable z . In addition, due to the condensed latent space, Bayesian cyclic model with sampled SFM achieves a more stable status than that with $z^{(i)}$ in training process.

For better understanding the difference between the original model and Bayesian CycleCAN, we propose an integrated cyclic framework by introducing a balance factor γ , the coefficient of adversarial loss in reconstructed ends which has two helpful functions: first, it enhances the reconstructed learning and boosts realistic color distribution; second, it effects the stability of cyclic model by accelerating the learning process of discriminators. We evaluate the performances of both models under different values of γ .

The main contributions of our work are summarized as:

- We propose a novel model called Bayesian CycleGAN for unsupervised learning by exploring the full posteriors of Bayesian cyclic model (with latent sampling).
- We impose restriction on the latent space for generating diversified images by adding encoder networks.
- We introduce a hyper-parameter for better balancing the reconstructed learning and training stability, and prove this variation also has a global optimum.
- We perform experiments on several datasets, demonstrating that the proposed model confers a defense against instability and outperform the original model.

2. Related Works

Image-to-Image Translation Image-to-Image translation is a classical problem in computer vision. Motivated by the success of generative model like Generative Adversarial Networks [6], our focus has begun to change from one selected artwork style transfer to inter-domain translation. For supervised learning, conditional GANs has been used in Pix2pix [11] to convert images from one domain to another, like landscapes to semantic labels. Also, BicycleGAN [28] is the enhanced version of Pix2pix since it generated diversified outputs. Besides, VAE is a probabilistic model with an encoder to map images to a latent representation and a decoder to reconstruct the images, which can also be used in inter-domain translation. We adopt a VAE-like network to generate the restricted latent sampling, but there are two main differences: first, our network replaces the encoder/decoder to down/up sample layers; second, we abolish the l_1 loss between reconstructed image and source image. For unsupervised learning, there has been a recent surge on cyclic GANs [27, 17, 16, 25, 24], which aim to

learn a joint distribution given marginal distribution in each individual domain. Zhu et al. presented CycleGAN to learn mappings between different domains without paired data, achieving good results [27]. Almahairi et al. presented the augmented many-to-many mapping method based on CycleGAN, taking Gaussian noise into another cycle with GAN loss and l_1 loss restrained and training normal cycle along with the latent cycle [1]. Different from our work, augmented CycleGAN directly target many-to-many mappings.

GANs stability Although GANs has achieved excellent results in many research areas, the training process is still intractable for its weak stability. Many recent works have focused on changing the objectives of GAN training [20, 18, 2, 15, 7, 19, 26]. The work in Bayesian GAN [22], however, explores the Bayesian formulation for model network parameters and conducts posteriors inference to improve stability and solve model collapse of GAN training.

The Bayesian GAN [22] is the most related one to ours. There are two main differences between them: first, instead of generating predictive distribution with random variable z , our Bayesian posteriors are based on cyclic framework, mapping between different domains; second, Bayesian GAN performs posteriors sampling in iteration process while our model adopts iterative MAP optimization along with latent sampling due to the practical nature of cyclic model. Compared with the original CycleGAN [27], Bayesian cyclic model implements the Bayesian extension with Gaussian prior for original cyclic model in theory; secondly, it is optimized with MAP and latent sampling, bringing robustness improvement via the inductive bias, while the optimizing process of original cyclic model is the maximum likelihood estimation (MLE); finally, in addition to one-to-one mapping, Bayesian cyclic model can generate diversified images by imposing restriction on the latent variable.

3. Proposed Method

In this section, we describe the architecture of Bayesian CycleGAN. We first deduce the Bayesian formulation based on integrated cyclic framework, in which the balance factor, γ , is introduced. Then we formulate the Bayesian cyclic model with marginalizing latent sampling over the whole posteriors. Finally, we impose restriction on latent space for diversified generating.

3.1. Bayesian Extension for CycleGAN

Given two domains X and Y with associated datasets $\mathcal{X} = \{x^{(i)}\}$ and $\mathcal{Y} = \{y^{(j)}\}$, the goal is to fit distribution $p_Y(y)$ based on given $p_X(x)$ using generator $G_A(x; \theta_{ga})$, parametrized by θ_{ga} , and reconstruct $p_X(x)$ by feeding y through the inverse generator $G_B(y; \theta_{gb})$, parametrized by θ_{gb} . Cyclic model estimates the parameters of generators

by satisfying two constraints: marginal matching and cycle-consistency. Marginal matching means the generated images close to the true distribution in target domain. Cycle-consistency prevents the reconstructed results from contradicting source domain, without which the cyclic model could not work normally.

Now we analyze the judgement view of discriminators. For the sake of clarity, we denote $G_A(x; \theta_{ga})$ as \tilde{y} and $G_A(G_B(y; \theta_{gb}); \theta_{ga})$ as \hat{y} , similar notations are used for x , \tilde{x} and \hat{x} . In the integrated cyclic framework, shown in Figure 1, we are able to access three parts of the distribution $p_Y(y)$, using for training the discriminator D_A : $(y, t = 1)$, $(\tilde{y}, t = 0)$ and $(\hat{y}, t = 0)$, in which t are the labels for discrimination. The conditional likelihoods are defined as:

$$p(t = 1|X, Y, Z_y = y, \theta_{da}, \theta_g) \propto D_A(y; \theta_{da}) \quad (1)$$

$$p(t = 0|X, Y, Z_y = \tilde{y}, \theta_{da}, \theta_g) \propto 1 - D_A(\tilde{y}; \theta_{da}) \quad (2)$$

$$p(t = 0|X, Y, Z_y = \hat{y}, \theta_{da}, \theta_g) \propto 1 - D_A(\hat{y}; \theta_{da}) \quad (3)$$

The auxiliary variable is noted as $Z_y \in \{y, \tilde{y}, \hat{y}\}$. Here Z_y is a multinomial distribution for indicating the input assignments. Assume the ratio between number of pairs $|\{(y, t)\}| : |\{(\tilde{y}, t)\}| : |\{(\hat{y}, t)\}| = 1 + \gamma : 1 : \gamma$, where γ is the introduced balance factor, indicating the coefficient of adding adversarial loss in reconstructed ends. The balance factor can be viewed as zero in original cyclic framework since there is only l_1 loss constraint in reconstructed ends. We prove that this variation also has a global optimum theoretically in Appendix A.2, and show that the balance factor can adjust model stability as well as enhance reconstructed learning in experiments.

For Bayesian cyclic model, instead of performing posteriors sampling in iteration process like Bayesian GAN, we employ variant-concatenate inputs and regularized priors to formulate full posteriors due to the practical nature of cyclic model mentioned in [1]. By concatenating the input images, like x , and sampled latent Gaussian random variable $z^{(j)}$, $j = 1, 2 \dots m_x$ to construct a set of input $x_z^{(j)}$, we are able to formulate full posteriors and then update networks' parameters with Maximum a posterior estimation. To articulate the posteriors of integrated cyclic framework (with balance factor), we infer different sampled space that posteriors conditioned on: $\Omega_g = (x, y, x_z, y_z)$, $\Omega_{da} = (x, y, Y, x_z, y_z)$, and $\Omega_{db} = (x, y, X, x_z, y_z)$. Therefore, the posterior of discriminator θ_{da} for each sampled x_z can be derived as (we use \propto for convenient expression):

$$\begin{aligned} & p(\theta_{da}|\Omega_{da}, t, \theta_{ga}, \theta_{gb}) \\ & \propto (D_A(y; \theta_{da}))^{(1+\gamma)} \times (1 - D_A(\tilde{y}; \theta_{da}))^\gamma \quad (4) \\ & \times (1 - D_A(G_A(x_z; \theta_{ga}); \theta_{da})) \times p(\theta_{da}|\alpha_{da}). \end{aligned}$$

$p(\theta_{da}|\alpha_{da})$ is regularized prior over discriminator D_A in which α means hyper-parameters for D_A . Other posteriors for θ_{db} and θ_g can be derived analogously.

3.2. Bayesian Marginalization

We use Bayesian marginalization to get rid of Ω defining on training set, in which way we can apply the estimated parameters to do inference without distortion theoretically. Here we display the marginalization process, taking posterior $p(\theta_{da}|\Omega_{da}, t, \theta_{ga}, \theta_{gb})$ for example:

$$\begin{aligned} & p(\theta_{da}|t, \theta_{ga}, \theta_{gb}) \\ & = \int p(\theta_{da}, \Omega_{da}|t, \theta_{ga}, \theta_{gb}) d\Omega_{da} \\ & = \int p(\theta_{da}|\Omega_{da}, t, \theta_{ga}, \theta_{gb}) \cdot p(\Omega_{da}|\theta_{ga}, \theta_{gb}) d\Omega_{da} \\ & = \int p(\theta_{da}|\Omega_{da}, t, \theta_g) \cdot p(x, y, x_z, y_z) \cdot p(Y|x, y, x_z, y_z) d\Omega_{da} \\ & = \sum_{i=1}^{n_x} \sum_{j=1}^{n_y} \sum_{k=1}^{m_y} \sum_{l=1}^{m_x} p(\theta_{da}|\Omega_{da}, t, \theta_{ga}, \theta_{gb}), \end{aligned}$$

in which n_x, n_y represents batch size for training process; m_x, m_y mean latent sampling number. Built upon over above derivation, the posterior for θ_{da} can be rewritten as:

$$\begin{aligned} & p(\theta_{da}|t, \theta_{ga}, \theta_{gb}) \\ & \propto \prod_{j=1}^{n_y} (D_A(y^{(j)}; \theta_{da}))^{(1+\gamma)m_x} \times \prod_{j=1}^{n_y} \prod_{l=1}^{m_x} (1 - D_A(\hat{y}^{(j,l)}; \theta_{da}))^\gamma \\ & \times \prod_{i=1}^{n_x} \prod_{k=1}^{m_y} (1 - D_A(G_A(x_z^{(i,k)}; \theta_{ga}); \theta_{da})) \times p(\theta_{da}|\alpha_{da}). \quad (5) \end{aligned}$$

Similarly, we can derive the posterior for θ_{db} to be

$$\begin{aligned} & p(\theta_{db}|t, \theta_{ga}, \theta_{gb}) \\ & \propto \prod_{i=1}^{n_x} (D_B(x^{(i)}; \theta_{db}))^{(1+\gamma)m_y} \times \prod_{i=1}^{n_x} \prod_{k=1}^{m_y} (1 - D_B(\hat{x}^{(i,k)}; \theta_{db}))^\gamma \\ & \times \prod_{j=1}^{n_y} \prod_{l=1}^{m_x} (1 - D_B(G_B(y_z^{(j,l)}; \theta_{gb}); \theta_{db})) \times p(\theta_{db}|\alpha_{db}). \quad (6) \end{aligned}$$

For the estimation of generators' parameters, we generate the data pairs by flipping the label t , with the same conditional likelihood defined above, we are then able to get the posterior with the cycle consistency constraints:

$$\begin{aligned} & p(\theta_{ga}, \theta_{gb}|\theta_{da}, \theta_{db}) \\ & \propto \left(\prod_{i=1}^{n_x} \prod_{k=1}^{m_y} D_A(G_A(x_z^{(i,k)})) \times (D_B(\hat{x}^{(i,k)}))^\gamma \cdot e^{-\lambda \|\hat{x}^{(i,k)} - x^{(i)}\|} \right) \\ & \times \left(\prod_{j=1}^{n_y} \prod_{l=1}^{m_x} D_B(G_B(y_z^{(j,l)})) \times (D_A(\hat{y}^{(j,l)}))^\gamma \cdot e^{-\lambda \|\hat{y}^{(j,l)} - y^{(j)}\|} \right) \\ & \times p(\theta_{ga}|\alpha_{ga}) \times p(\theta_{gb}|\alpha_{gb}). \quad (7) \end{aligned}$$

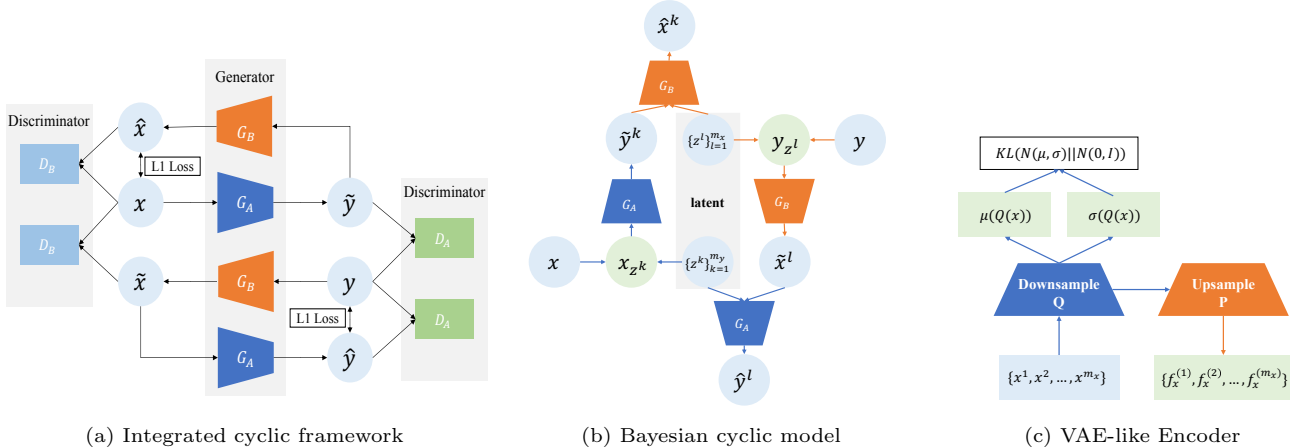


Figure 1. (a) Integrated cyclic framework: We explore the integrated cyclic framework by adding GAN loss between reconstructed image and source image, taking γ as the coefficient. (b) Bayesian cyclic model: We deduce the full posteriors over parameters and adopt iterative MAP optimization along with the latent sampling to update networks. (c) VAE-like Encoder: We use this encoder to generate SFM latent variable which can be replaced in the inference process to get diversified outputs.

To reduce model oscillation, we follow the original cyclic model and replace the negative log likelihood objective by a least square loss. We formulate the alternative using the combination of l_1 and least square adversarial loss in Bayesian cyclic model, whose derivations is the same as above formulation for standard adversarial loss. That detailed formulation of posteriors with l_1 -least square adversarial loss are shown in Appendix A.1.

3.3. SFM Latent Sampling

Original cyclic model cannot realize multi-objective mapping with stochastic variable z due to the fundamental flaw of cyclic framework: the cycle-consistency encourages the mapping to ignore the latent z [1]. Thinking outside the square, we can use only one part of latent space to fit in training process and therefore, it is possible for us to generate diversified images in the inference process by replacing the restricted latent variable with samples form other latent distributions. In our implementation, we use VAE-like encoder network to generate the latent *statistic feature map* (SFM) $f_x^{(j)} \sim E(x)$, which remains much the same for each domain. We show the diversified effect in the Monet2Photo part of experiments by replacing SFM to other latent variables. Furthermore, due to the smaller latent space in training process, Bayesian cyclic model achieves a more stable status compared with latent $z^{(j)}$. We use this trick in the following experiments.

The VAE-like network E is illustrated in Figure 1, it has down-sample layers Q , up-sample layers P , which is the first difference from VAE composed of encoder and decoder. And it is restricted with the \mathcal{KL} loss lying in the bottleneck layer between Q and P , that encourage outputs close to Gaussian distribution since we do not want our en-

coder make $f_x \sim E_A(x)$ more dominant than y , in which case G_B translate from y_f , concatenate input of y and f_x , to x rather than \tilde{x} corresponding to y . This is the second difference from VAE which uses l_1 loss between reconstructed images and source images to generate realistic images.

The new Bayesian formulation with SFM latent sampling is similar to that cyclic model with Gaussian random latent sampling. We only need to replace z with $f_{x/y}$ and remain other parts fixed.

3.4. Practical Implementation Algorithm

We marginalize the posteriors over generators and discriminators shown in Equations 5, 6 and 7, which are all responsible for optimization and accompanied by a regularization item as prior $p(\theta|\alpha)$. Detailed procedures of the optimization for each iteration are shown in Appendix A.5.

4. Experiments

We first describe the used benchmark datasets and implementation details. Then we perform comparison among original cyclic model, Bayesian cyclic model and several variants, and analysis how them support for our claims respectively. In addition, we show the enhanced reconstructed learning effect caused by the introduction of balance factor, and the diversified effect resulting from replacing the restricted latent variables during inference process.

4.1. Dataset

We evaluate the proposed Bayesian cyclic model on three widely used benchmarks, Cityscapes [3], Maps and Monet2Photo [27]. We use Cityscapes for mapping learning between realistic photos and semantic labels, with 2975 training images from training set and 500 testing images

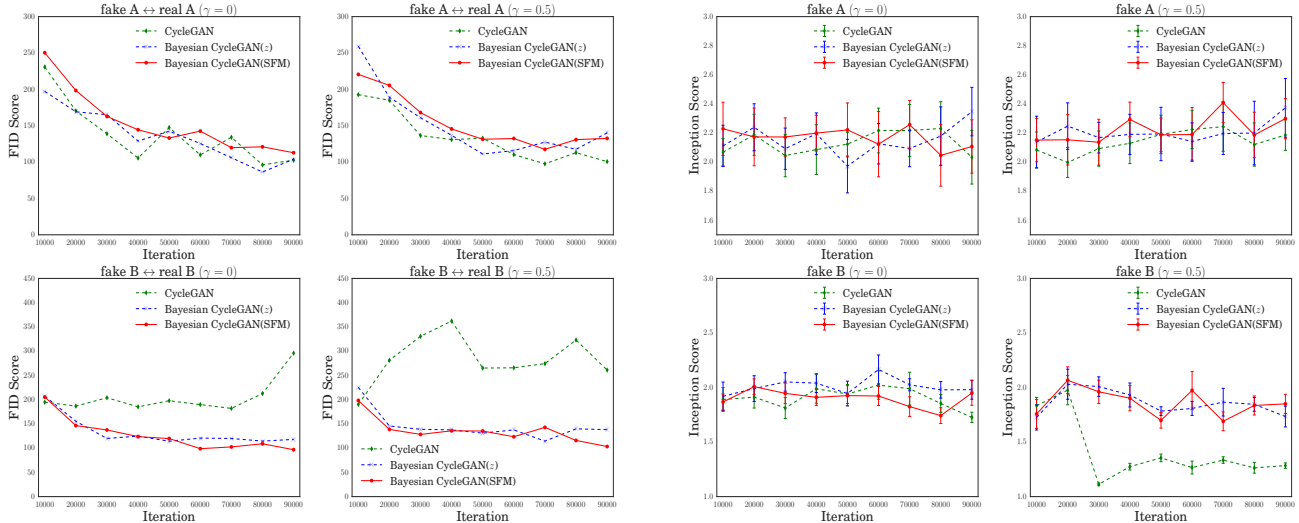


Figure 2. Left: FID scores estimate the *distance* between source images and generated ones in different iterations. Right: Inception scores of different iterations with mean value and standard deviation. *A* represents the streetscapes; *B* signifies semantic segmentation labels.

from validation set. Each picture is resized to 128×256 . We use Maps for mapping learning between aerial photographs and maps scraped from Google Maps, with 1096 training images and 1098 testing images. Each picture is resized to 256×256 . We use Monet2Photo for mapping learning between landscapes and artworks (style transfer), with 1074 Monet artworks and 6853 landscapes.

4.2. Implementation Details

We employ the same network architectures for both the generator and discriminator and same hyper-parameters for training process. The generator consists of 6 basic residual blocks [8] between two down-sample layers and two up-sample layers, assembled by instance normalization. The discriminator consists of several convolutional layers. In the training process, we use ADAM [14] with learning rate 0.0002 for the first 50 epochs, the learning rate will non-linearly decay to zero periodically for the next 50 epochs, momentums were set as $\beta_1 = 0.5$ and $\beta_2 = 0.999$. Weights for networks are initialized as Gaussian distribution with zero mean and standard deviation 0.02. The other hyper-parameters, default values are $\lambda = 10$, $\lambda_{KL} = 0.1$. Besides, we set Monte Carlo latent sample numbers as 3 both for f_x and f_y for Bayesian marginalization.

4.3. Comparison via Standard Metrics

Photo ↔ label We evaluate different methods using FID score [9] and inception score [23] in original framework ($\gamma = 0$), the scores are illustrated in Figure 2, from which we find that various methods achieve similar performance for easy task *label* → *photo*. However, for semantic task *photo* → *label*, Bayesian cyclic models outperform original ones in both stability and quality.

Now, we take the balance factor of model stability into account. By adding adversarial loss in reconstructed ends, which is a good news and also a challenge for discriminators since reconstructed images distribute closer to truth data than generated ones under guarantee of L1 loss, crazy learning discriminators descent gradients fast and therefore, generators fail to keep pace with their rivals. In few epochs, the whole cyclic model collapses accompanied with discriminators' victory. In lieu of the unilateral victory, what we really expect is a win-win situation. Bayesian cyclic model enhances the generators training by employing variant-concatenate inputs and regularized priors, resistant to the crazy learning judgement. As shown in Figure 5 and 2, CycleGAN models already suffer from model collapse, generating identical and meaningless label maps regardless of the input streetscapes, while our Bayesian cyclic models remain stabilized mapping.

Although perceptual studies may be the gold standard for assessing graphical realism, we also adopt automatic quantitative FCN scores, the metrics from Cityscapes benchmark including per-pixel accuracy, per-class accuracy and mean IOU, for evaluating *photo* → *label* task. The results are shown in Table 1. Our Bayesian model outperforms the original one with or without introduced balance factor. In addition to the quantitative results, we provide some sampled qualitative results shown in Figure 4.

Aerial ↔ Maps We evaluate different methods using FID and inception score in Table 2, from which we find that the Bayesian cyclic model achieves better performances than original one. The qualitative results in Figure 7 demonstrate the realistic effect of proposed Bayesian cyclic model.

Monet ↔ Photo is a kind of image style transfer. Instead of focusing on the neural transfer [5] that mimic the style

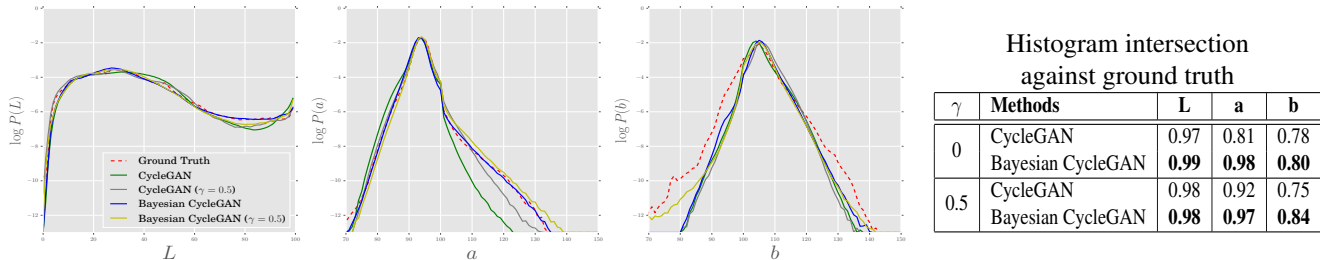


Figure 3. Left: Color distribution matching property of different methods, tested on Cityscapes. We show the log probability for emphasizing the differences in low probability regions. Right: Histogram intersection against ground truth.

of only one painting, we employ automatic mapping and compare different methods in Table 3.

γ	Methods	Per-pixel acc.	Per-class acc.	Class IOU
0	CycleGAN	0.48	0.18	0.11
	CycleGAN (dropout)	0.56	0.18	0.12
	CycleGAN (buffer)	0.58	0.22	0.16
	Bayesian CycleGAN	0.73	0.27	0.20
0.5	CycleGAN	0.45	0.11	0.07
	CycleGAN (dropout)	0.59	0.16	0.11
	Bayesian CycleGAN	0.65	0.20	0.15
	Pix2pix (Supervised)	0.85	0.40	0.32

Table 1. FCN-scores for different methods, evaluated on photo \rightarrow label. *Buffer* is the trick used by Zhu et al. For fair comparison, we evaluate all methods after 200 epochs.

γ	Methods	FID A	FID B	Inception A	Inception B
0	CycleGAN	71.56	172.75	3.50 \pm 0.25	2.77 \pm 0.14
	Bayesian CycleGAN	68.45	165.83	3.68\pm0.22	2.85\pm0.15
0.5	CycleGAN	77.92	198.26	3.43 \pm 0.11	2.56 \pm 0.16
	Bayesian CycleGAN	72.86	160.66	3.61\pm0.32	2.83\pm0.12

Table 2. Evaluation for Maps \leftrightarrow Aerial mapping. FID A evaluates statistic distance between generated aerial photos and real photos set, FID B is between generated maps and real maps set. Inception score evaluates the quality of generated images.

Methods	FID A	FID B	Inception A	Inception B
CycleGAN	155.32	140.00	3.76 \pm 0.73	3.17 \pm 0.35
Bayesian CycleGAN	151.24	137.74	3.86\pm0.64	3.35\pm0.34

Table 3. Evaluation for Monet \leftrightarrow Photo mapping. FID A evaluates statistic distance between generated images of Monet style and artworks; FID B is between generated photos and landscapes.

4.4. Boost Realistic Color Distribution

Another striking effect of Bayesian cyclic models is that they generate realistic landscapes with extensive color distribution. As demonstrated in [12], L1 loss stimulates an average, grayish color when it comes to uncertainty space, while adversarial loss encourages sharp and realistic color distribution. The sampling and regularized priors in our method enhance the sharpening effect of adversarial loss

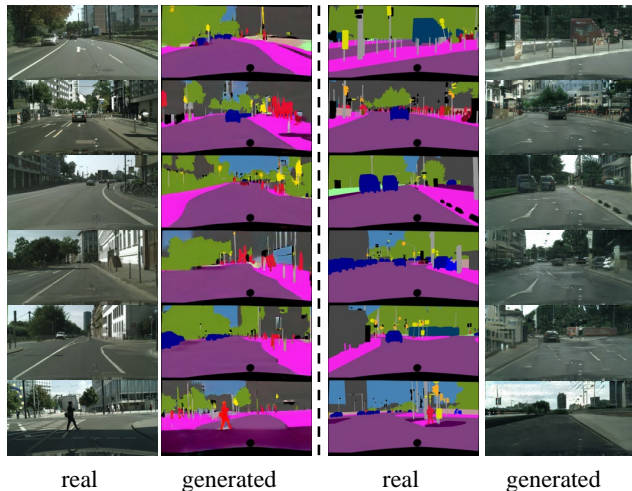


Figure 4. Qualitative results sampling from Bayesian cyclic model in unsupervised setting under condition $\gamma = 0$.

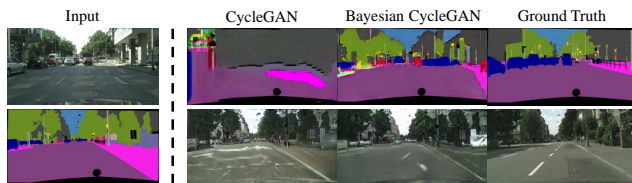


Figure 5. Comparison of stability: Results for mapping *label* \leftrightarrow *photo* trained on cityscapes under condition $\gamma = 0.5$.

in gradient descend process, which in turn make generated image more colorful. In addition, the introduced adversarial loss in reconstructed end also incentivize matching the true color distribution. In figure 3, we investigate if our Bayesian cyclic model actually achieve this effect on the Cityscapes dataset. The plots show the marginal distributions over generated color values in Lab color space. We find that a) Bayesian cyclic model generate almost unanimous La distribution with ground truth, and encourage broader b distribution than original methods. b) The introduced balance factor leads to a wider distribution, confirming the hypothesis that the Bayesian extension and introduced balance factor both contribute to generating closer color distribution.



Figure 6. We use different methods under different conditions for $label \leftrightarrow photo$ mapping. Then we infer reconstructed images after training 50000 iterations and calculate GDL between reconstructed image and source image. The results demonstrate that the introduction of γ enhances reconstructed learning.



Figure 7. Qualitative results for Maps \leftrightarrow Aerial conditioned on $\gamma = 0$.

4.5. Enhance Reconstructed Learning

We have shown the effect of balance factor γ on the stability of cyclic model. Since the GAN loss is added between real images and reconstructed images, which are more realistic than generated ones, the return gradients for generators are relatively smaller than that for discriminators so that the min-max adversarial game goes out of balance. That explains why original cyclic model suffers from model collapse as illustrated in Figure 5, and also demonstrate our Bayesian cyclic model is more stable. Now, we present the other function of γ : enhancing reconstructed learning.

In theory, by introducing the balance factor, the optimal status of cyclic model changes from $p_y(y) = p_{\bar{y}}(y)$ to $(1 + \gamma)p_y(y) = p_{\bar{y}}(y) + \gamma p_{\bar{y}}(y)$ (prove in Appendix A2/A3), which encourages the distribution of reconstructed images closer to real data distribution. In practice, we compare the FID scores of reconstructed distribution under different settings, illustrated in Figure 8. The FID scores for cyclic model conditioned on $\gamma = 0.5$ are lower compared with that conditioned on $\gamma = 0$, which means the balance factor enhances reconstructed learning.

In addition, we exhibit reconstructed images from the perspective of qualitative analysis and evaluate the images with GDL, Gradient Difference Loss [4], shown in Figure 6. In which lower GDL means that the reconstructed images create a sense of verisimilitude and have similar semantic expression with real images. The GDL scores show our Bayesian cyclic model conditioned on $\gamma = 0.5$ achieves the best performance.

4.6. Diversify Outputs by Replacing SFM

As mentioned in [1], stochastic CycleGAN cannot generate diversified outputs since the cycle-consistency loss encourages the mapping to ignore latent z . To generate diversified outputs, we can divide latent space into various parts and use only one particular part to fit in training process. In the inference process, we can diversify generate outputs

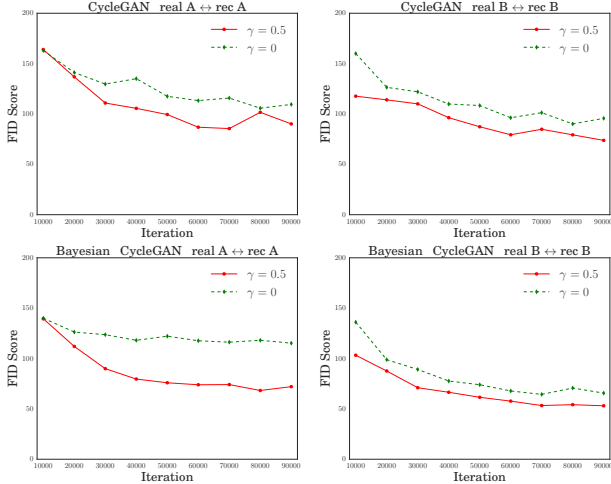


Figure 8. The FID scores estimate *distance* between the distribution of source images and that of reconstructed images generated by original cyclic model / Bayesian cyclic model.



Figure 9. Translation of Monet \leftrightarrow Photo: The left column are source images, middle column are generated ones, right columns are diversified outputs generated by replacing SFM with other latent variables, shown on the lower right corner of pictures.

by replacing that part with another latent distribution. In our implementation, we impose the restriction on sampled latent space by changing the latent variable from random noise z to SFM generated by VAE-like network. By replacing the SFM with other latent variable, the cyclic model can generate diversified outputs. We carry out several tests on *monet* \leftrightarrow *photo* style transfer experiment. The diversified outputs and corresponding latent variables are shown in Figure 9.

5. Adaptability to Semi-Supervised Setting

In cases where paired data is accessible, we can leverage the supervision to train our model in a semi-supervised setting. By doing this, we could get more accurate mapping in several complicated scenario. In the training process of Cityscapes, mapping errors often occur, for example, the initial model cannot recognize trees, thus, translating trees

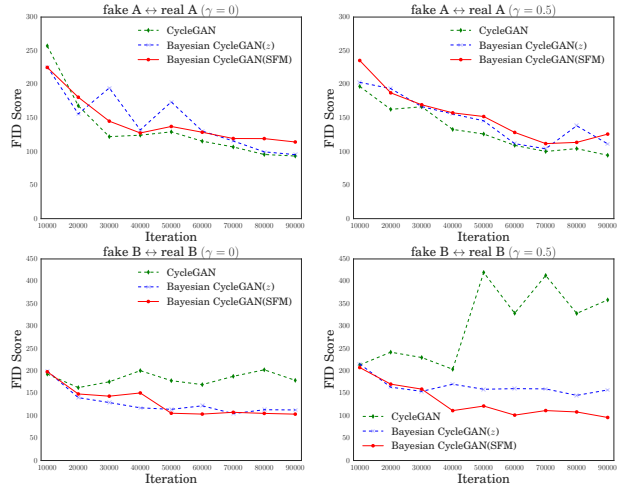


Figure 10. Quantitative results for semi-supervised learning. The FID scores estimate the *distance* between the distribution of real images and that of generated ones. The analysis and conclusion in semi-supervised setting are similar with Section 4.3.

into something else due to the unsupervised setting. To resolve these ambiguities requires weak semantic supervision, we can use 30 (around 1%) paired data (pictures of cityscape and corresponding label images) to initialize our model at the beginning for each epoch. The results (Figure 10) show that our model still outperforms the baselines. We also find that adding slight prior knowledge increases the accuracy of mapping between photos and labels significantly.

6. Conclusion

In this paper, we propose a Bayesian extension of cyclic model and an integrated cyclic framework for inter-domain mapping. By exploring the whole posteriors of the Bayesian cyclic model with latent sampling and regularized priors, Bayesian CycleGAN can enhance the generators and therefore reduce the risk of model collapse and instability caused by the unbalance of min-max optimization game. This is an explanation why we achieved more stable training and better domain-to-domain translation results. In the meantime, the proposed integrated cyclic framework enable realistic reconstructed learning in theory and practice by replacing the l_1 loss with a combination of l_1 -GAN loss. In addition, after imposing restriction on the sampled latent variables, we can achieve diversified mappings by replacing the SFM with other latent variables in inference process.

The plan of our research orientation is how to achieve controllable many-to-many mapping under this framework. Also, modify prior models according to dynamic posterior estimation is worthy of future research.

References

- [1] A. Almahairi, S. Rajeswar, A. Sordoni, P. Bachman, and A. Courville. Augmented cyclegan: Learning many-to-many mappings from unpaired data. *arXiv preprint arXiv:1802.10151*, 2018. [1](#), [2](#), [3](#), [4](#), [7](#)
- [2] M. Arjovsky, S. Chintala, and L. Bottou. Wasserstein gan. *arXiv preprint arXiv:1701.07875*, 2017. [2](#)
- [3] M. Cordts, M. Omran, S. Ramos, T. Rehfeld, M. Enzweiler, R. Benenson, U. Franke, S. Roth, and B. Schiele. The cityscapes dataset for semantic urban scene understanding. In *The IEEE Conference on Computer Vision and Pattern Recognition (CVPR)*, pages 3213–3223, 2016. [4](#)
- [4] C. Fabbri, M. J. Islam, and J. Sattar. Enhancing underwater imagery using generative adversarial networks. *arXiv preprint arXiv:1801.04011*, 2018. [7](#)
- [5] L. A. Gatys, A. S. Ecker, and M. Bethge. Image style transfer using convolutional neural networks. In *The IEEE Conference on Computer Vision and Pattern Recognition (CVPR)*, pages 2414–2423, 2016. [5](#)
- [6] I. Goodfellow, J. Pouget-Abadie, M. Mirza, B. Xu, D. Warde-Farley, S. Ozair, A. Courville, and Y. Bengio. Generative adversarial nets. In *Advances in Neural Information Processing Systems 27*, pages 2672–2680. 2014. [1](#), [2](#)
- [7] I. Gulrajani, F. Ahmed, M. Arjovsky, V. Dumoulin, and A. C. Courville. Improved training of wasserstein gans. In *Advances in Neural Information Processing Systems*, pages 5769–5779, 2017. [2](#)
- [8] K. He, X. Zhang, S. Ren, and J. Sun. Deep residual learning for image recognition. In *Proceedings of the IEEE conference on computer vision and pattern recognition*, pages 770–778, 2016. [5](#)
- [9] M. Heusel, H. Ramsauer, T. Unterthiner, B. Nessler, and S. Hochreiter. Gans trained by a two time-scale update rule converge to a local nash equilibrium. In *Advances in Neural Information Processing Systems*, pages 6629–6640, 2017. [5](#)
- [10] X. Huang, M.-Y. Liu, S. Belongie, and J. Kautz. Multimodal unsupervised image-to-image translation. In *The European Conference of Computer Vision (ECCV)*, 2018. [1](#)
- [11] P. Isola, J.-Y. Zhu, T. Zhou, and A. A. Efros. Image-to-image translation with conditional adversarial networks. In *IEEE Conference on Computer Vision and Pattern Recognition (CVPR)*, pages 1125–1134, 2017. [2](#)
- [12] P. Isola, J.-Y. Zhu, T. Zhou, and A. A. Efros. Image-to-image translation with conditional adversarial networks. *The IEEE Conference on Computer Vision and Pattern Recognition (CVPR)*, 2017. [6](#)
- [13] T. Kim, M. Cha, H. Kim, J. K. Lee, and J. Kim. Learning to discover cross-domain relations with generative adversarial networks. In D. Precup and Y. W. Teh, editors, *Proceedings of the 34th International Conference on Machine Learning*, volume 70 of *Proceedings of Machine Learning Research*, pages 1857–1865, International Convention Centre, Sydney, Australia, 06–11 Aug 2017. PMLR. [1](#)
- [14] D. P. Kingma and J. Ba. Adam: A method for stochastic optimization. In *International Conference on Learning Representations*, 2015. [5](#)
- [15] C.-L. Li, W.-C. Chang, Y. Cheng, Y. Yang, and B. Póczos. Mmd gan: Towards deeper understanding of moment matching network. In *Advances in Neural Information Processing Systems*, pages 2200–2210, 2017. [2](#)
- [16] M.-Y. Liu, T. Breuel, and J. Kautz. Unsupervised image-to-image translation networks. In *Advances in Neural Information Processing Systems*, pages 700–708, 2017. [1](#), [2](#)
- [17] M.-Y. Liu and O. Tuzel. Coupled generative adversarial networks. In *Advances in Neural Information Processing Systems*, pages 469–477, 2016. [1](#), [2](#)
- [18] X. Mao, Q. Li, H. Xie, R. Y. Lau, Z. Wang, and S. P. Smolley. Least squares generative adversarial networks. In *The IEEE International Conference on Computer Vision (ICCV)*, pages 2813–2821. IEEE, 2017. [2](#)
- [19] Y. Mroueh, C.-L. Li, T. Sercu, A. Raj, and Y. Cheng. Sobolev gan. *arXiv preprint arXiv:1711.04894*, 2017. [2](#)
- [20] S. Nowozin, B. Cseke, and R. Tomioka. f-gan: Training generative neural samplers using variational divergence minimization. In *Advances in Neural Information Processing Systems*, pages 271–279, 2016. [2](#)
- [21] A. Royer, K. Bousmalis, S. Gouws, F. Bertsch, I. Mosseri, F. Cole, and K. Murphy. XGAN: unsupervised image-to-image translation for many-to-many mappings. *CoRR*, abs/1711.05139, 2017. [1](#)
- [22] Y. Saatchi and A. G. Wilson. Bayesian gan. In *Advances in Neural Information Processing Systems*, pages 3622–3631, 2017. [1](#), [2](#)
- [23] T. Salimans, I. Goodfellow, W. Zaremba, V. Cheung, A. Radford, and X. Chen. Improved techniques for training gans. In *Advances in Neural Information Processing Systems*, pages 2234–2242, 2016. [5](#)
- [24] Y. Taigman, A. Polyak, and L. Wolf. Unsupervised cross-domain image generation. In *International Conference on Learning Representations*, 2016. [2](#)
- [25] Z. Yi, H. Zhang, P. Tan, and M. Gong. Dualgan: Unsupervised dual learning for image-to-image translation. In *The IEEE International Conference on Computer Vision (ICCV)*, 2017. [1](#), [2](#)
- [26] S. Zhai, Y. Cheng, R. S. Feris, and Z. Zhang. Generative adversarial networks as variational training of energy based models. *CoRR*, abs/1611.01799, 2016. [2](#)
- [27] J.-Y. Zhu, T. Park, P. Isola, and A. A. Efros. Unpaired image-to-image translation using cycle-consistent adversarial networks. In *The IEEE International Conference on Computer Vision (ICCV)*, 2017. [1](#), [2](#), [4](#)
- [28] J.-Y. Zhu, R. Zhang, D. Pathak, T. Darrell, A. A. Efros, O. Wang, and E. Shechtman. Toward multimodal image-to-image translation. In I. Guyon, U. V. Luxburg, S. Bengio, H. Wallach, R. Fergus, S. Vishwanathan, and R. Garnett, editors, *Advances in Neural Information Processing Systems 30*, pages 465–476. Curran Associates, Inc., 2017. [2](#)

A. Supplementary Material for Bayesian CycleGAN

A.1. Model with Least Square GAN loss

The posteriors over generators and discriminators of Bayesian cyclic model with *Least Square* GAN loss can be deduced as:

$$p(\theta_{da}|t, \theta_{ga}, \theta_{gb}) \propto \left(\prod_{j=1}^{n_y} e^{-(1+\gamma) \cdot m_x \cdot (D_A(y^{(j)}; \theta_{da}) - 1)^2} \cdot \prod_{j=1}^{n_y} \prod_{l=1}^{m_x} e^{-\gamma \cdot (D_A(\hat{y}^{(j,l)}; \theta_{da}))^2} \right) \times \left(\prod_{i=1}^{n_x} \prod_{k=1}^{m_y} e^{-(D_A(G_A(x_z^{(i,k)}; \theta_{ga}); \theta_{da}))^2} \right) \times p(\theta_{da}|\alpha_{da}) \quad (8)$$

$$p(\theta_{db}|t, \theta_{ga}, \theta_{gb}) \propto \left(\prod_{i=1}^{n_x} e^{-(1+\gamma) \cdot m_y \cdot (D_B(x^{(i)}; \theta_{db}) - 1)^2} \cdot \prod_{i=1}^{n_x} \prod_{k=1}^{m_y} e^{-\gamma \cdot (D_B(\hat{x}^{(i,k)}; \theta_{db}))^2} \right) \times \left(\prod_{j=1}^{n_y} \prod_{l=1}^{m_x} e^{-(D_B(G_B(y_z^{(j,l)}; \theta_{gb}); \theta_{db}))^2} \right) \times p(\theta_{db}|\alpha_{db}) \quad (9)$$

$$p(\theta_{ga}, \theta_{gb}|\theta_{da}, \theta_{db}) \propto \left(\prod_{i=1}^{n_x} \prod_{k=1}^{m_y} e^{-(D_A(G_A(x_z^{(i,k)}; \theta_{ga}); \theta_{da}) - 1)^2 - \gamma (D_B(\hat{x}^{(i,k)}; \theta_{db}) - 1)^2 - \lambda \|\hat{x}^{(i,k)} - x^{(i)}\|} \right) \times \left(\prod_{j=1}^{n_y} \prod_{l=1}^{m_x} e^{-(D_B(G_B(y_z^{(j,l)}; \theta_{gb}); \theta_{db}) - 1)^2 - \gamma (D_A(\hat{y}^{(j,l)}; \theta_{da}) - 1)^2 - \lambda \|\hat{y}^{(j,l)} - y^{(j)}\|} \right) \times p(\theta_{ga}|\alpha_{ga}) \times p(\theta_{gb}|\alpha_{gb}) \quad (10)$$

A.2. Global Optimality of Model with standard GAN loss

Proposition 1. For any given generator G_A and G_B , the optimal discriminator D_A (D_B can be deduced analogously) comes in the following form:

$$D_A^*(y) = \frac{(1 + \gamma)p_y(y)}{(1 + \gamma)p_y(y) + p_{\hat{y}}(y) + \gamma p_{\hat{y}}(y)} \quad (11)$$

Proof. We use posterior item $p(\theta_{da}|t, \theta_{ga}, \theta_{gb})$ to optimize D_A , aiming to maximum a posterior estimate, which can be defined as Equation (5). For convenience, we use the alternative posterior form which has the same meaning with original formula:

$$p(\theta_{da}|t, \theta_{ga}, \theta_{gb}) \approx \sum_{k=1}^{m_y} \sum_{l=1}^{m_x} \left(\sum_{i=1}^{n_x} \sum_{j=1}^{n_y} p(\theta_{da}|\Omega_{da}, \theta_{ga}, \theta_{gb}) \right) \sum_{i=1}^{n_x} \sum_{j=1}^{n_y} p(\theta_{da}|\Omega_{da}, \theta_{ga}, \theta_{gb}) \propto \prod_{j=1}^{n_y} (D_A(y^{(j)}; \theta_{da}))^{(1+\gamma)} \times \prod_{j=1}^{n_y} (1 - D_A(\hat{y}_z^{(j)}; \theta_{da}))^\gamma \times \prod_{i=1}^{n_x} (1 - D_A(G_A(x_z^{(i)}; \theta_{ga}); \theta_{da})) \times p(\theta_{da}|\alpha_{da}),$$

Due to Monte Carlo sampling methods has absolutely no effect on our proof, The optimization of $p(\theta_{da}|t, \theta_{ga}, \theta_{gb})$ equals to the optimization of $\sum_{i=1}^{n_x} \sum_{j=1}^{n_y} p(\theta_{da}|\Omega_{da}, \theta_{ga}, \theta_{gb})$, maximizing the quantity $V(G_A, G_B, D_A)$:

$$\max_{D_A} \log \left(\prod_{i=1}^{n_y} (D_A(y^{(i)}; \theta_{da}))^{1+\gamma} \times \prod_{i=1}^{n_x} (1 - D_A(G_A(x^{(i)}; \theta_{ga}); \theta_{da})) \times \prod_{i=1}^{n_y} (1 - D_A(\hat{y}^{(i)}; \theta_{da}))^\gamma \right),$$

which can be expressed as:

$$\begin{aligned} & (1 + \gamma) \cdot \mathbb{E}_{y \sim p_y(y)}[\log(D_A(y))] + \mathbb{E}_{y \sim p_{\tilde{y}}(y)}[\log(1 - D_A(y))] + \gamma \cdot \mathbb{E}_{y \sim p_{\hat{y}}(y)}[\log(1 - D_A(y))] \\ &= \int_y p_y(y)(1 + \gamma) \log(D_A(y)) + p_{\tilde{y}}(y) \log(1 - D_A(y)) + p_{\hat{y}}(y) \gamma \log(1 - D_A(y)) dy. \end{aligned}$$

The function $a(1 + \gamma) \log(y) + b \log(1 - y) + c \gamma \log(1 - y)$ achieves its maximum in $[0, 1]$ at $\frac{(1 + \gamma)a}{(1 + \gamma)a + b + \gamma c}$, so the integral function achieve the maximum at D_A^* . \square

We want to maximize the posterior of generators, which is equivalent to minimize the posterior of two discriminators and minimize the L1 term $\|\hat{y} - y\|, \|\hat{x} - x\|$ simultaneously. The following lemma shows the conditions of global optimality.

Lemma 1. *The global minimum of the training criterion $C(G) + L1$ can be achieved if and only if $p_y(y) = p_{\tilde{y}}(y) = p_{\hat{y}}(y)$ and $p_x(x) = p_{\tilde{x}}(x) = p_{\hat{x}}(x)$.*

Proof.

$$\begin{aligned} C(G) &= \max_{D_A} V(G_A, G_B, D_A) + \max_{D_B} V(G_A, G_B, D_B) \\ &= (1 + \gamma) \cdot \mathbb{E}_{y \sim p_y(y)}[\log(D_A^*(y))] + \mathbb{E}_{y \sim p_{\tilde{y}}(\tilde{y})}[\log(1 - D_A^*(y))] + \gamma \cdot \mathbb{E}_{y \sim p_{\hat{y}}(\hat{y})}[\log(1 - D_A^*(y))] \\ &\quad + (1 + \gamma) \cdot \mathbb{E}_{x \sim p_x(x)}[\log(D_B^*(x))] + \mathbb{E}_{x \sim p_{\tilde{x}}(\tilde{x})}[\log(1 - D_B^*(x))] + \gamma \cdot \mathbb{E}_{x \sim p_{\hat{x}}(\hat{x})}[\log(1 - D_B^*(x))] \\ &= (1 + \gamma) \sum p_y \log\left(\frac{(1 + \gamma)p_y}{(1 + \gamma)p_y + p_{\tilde{y}} + \gamma p_{\hat{y}}}\right) + \sum (p_{\tilde{y}} + \gamma p_{\hat{y}}) \log\left(\frac{p_{\tilde{y}} + \gamma p_{\hat{y}}}{(1 + \gamma)p_y + p_{\tilde{y}} + \gamma p_{\hat{y}}}\right) \\ &\quad + (1 + \gamma) \sum p_x \log\left(\frac{(1 + \gamma)p_x}{(1 + \gamma)p_x + p_{\tilde{x}} + \gamma p_{\hat{x}}}\right) + \sum (p_{\tilde{x}} + \gamma p_{\hat{x}}) \log\left(\frac{p_{\tilde{x}} + \gamma p_{\hat{x}}}{(1 + \gamma)p_x + p_{\tilde{x}} + \gamma p_{\hat{x}}}\right) \end{aligned}$$

When the condition is tenable, L1 term is zero. We rewrite the $C(G)$ equation with Kullback-Leibler divergence form and deduce that the minimum value of $C(G)$ is $-4(1 + \gamma) \log 2$.

$$\begin{aligned} C(G) &= -2(1 + \gamma) \log 2 - 2(1 + \gamma) \log 2 \\ &\quad + KL\left((1 + \gamma)p_y \left\| \frac{(1 + \gamma)p_y + p_{\tilde{y}} + \gamma p_{\hat{y}}}{2} \right\|\right) + KL\left(p_{\tilde{y}} + \gamma p_{\hat{y}} \left\| \frac{(1 + \gamma)p_y + p_{\tilde{y}} + \gamma p_{\hat{y}}}{2} \right\|\right) \\ &\quad + KL\left((1 + \gamma)p_x \left\| \frac{(1 + \gamma)p_x + p_{\tilde{x}} + \gamma p_{\hat{x}}}{2} \right\|\right) + KL\left(p_{\tilde{x}} + \gamma p_{\hat{x}} \left\| \frac{(1 + \gamma)p_x + p_{\tilde{x}} + \gamma p_{\hat{x}}}{2} \right\|\right) \\ &= -4(1 + \gamma) \log 2 + 2 \cdot JSD((1 + \gamma)p_y \parallel (p_{\tilde{y}} + \gamma p_{\hat{y}})) + 2 \cdot JSD((1 + \gamma)p_x \parallel (p_{\tilde{x}} + \gamma p_{\hat{x}})) \end{aligned}$$

According to the property of Jensen-Shannon divergence, which is always non-negative. The JSD can be zero only when that two distribution equal, that is $(1 + \gamma)p_y(y) = p_{\tilde{y}}(y) + \gamma p_{\hat{y}}(y)$ and $(1 + \gamma)p_x(x) = p_{\tilde{x}}(x) + \gamma p_{\hat{x}}(x)$. Then take the L1 term into consideration, if we want that achieve its minimum, there must be $p_{\tilde{y}} = p_y$ and $p_{\tilde{x}} = p_x$, so the global minimum of training criterion $C(G) + L1$ can be achieved if and only if $p_y(y) = p_{\tilde{y}}(y) = p_{\hat{y}}(y)$ and $p_x(x) = p_{\tilde{x}}(x) = p_{\hat{x}}(x)$. \square

A.3. Global Optimality of Model with Least Square GAN Loss

Proposition 2. *For any given generator G_A and G_B , the optimal discriminator D_A (D_B can be deduced analogously) comes in the following form:*

$$D_A^*(y) = \frac{(1 + \gamma)p_y(y)}{(1 + \gamma)p_y(y) + p_{\tilde{y}}(y) + p_{\hat{y}}(y)} \quad (12)$$

Proof. We use posterior item $p(\theta_{da}|t, \theta_{ga}, \theta_{gb})$ to optimize D_A , aiming to maximum a posterior estimate, due to the same reason as above proof for model with GAN loss, the optimization of $p(\theta_{da}|t, \theta_{ga}, \theta_{gb})$ equals to the optimization of $\sum_{i=1}^{n_x} \sum_{j=1}^{n_y} p(\theta_{da}|\Omega_{da}, \theta_{ga}, \theta_{gb})$, minimizing the quantity $V(G_A, G_B, D_A)$:

$$\max_{D_A} \log \left(\prod_{i=1}^{n_y} e^{-(1 + \gamma) \cdot (D_A(y^{(i)}; \theta_{da}) - 1)^2 - \gamma \cdot (D_A(\tilde{y}^{(i)}; \theta_{da}))^2} \times \prod_{i=1}^{n_x} e^{-(D_A(G_A(x^{(i)}; \theta_{ga}); \theta_{da}))^2} \right),$$

which can be expressed as:

$$\begin{aligned} V(G_A, G_B, D_A) &= (1 + \gamma) \cdot \mathbb{E}_{y \sim p_y(y)} [(D_A(y) - 1)^2] + \mathbb{E}_{y \sim p_{\tilde{y}}(y)} [(D_A(y))^2] + \gamma \cdot \mathbb{E}_{y \sim p_{\hat{y}}(y)} [(D_A(y))^2] \\ &= \int_y p_y(y)(1 + \gamma)(D_A(y) - 1)^2 + p_{\tilde{y}}(y)(D_A(y))^2 + p_{\hat{y}}(y)\gamma(D_A(y))^2 dy. \end{aligned}$$

The function $a(1 + \gamma)(y - 1)^2 + by^2 + c\gamma y^2$ achieves its minimum in $[0, 1]$ at $\frac{(1+\gamma)a}{(1+\gamma)a+b+\gamma c}$, so the integral function achieve the minimum value at D_A^* . \square

We want to maximize the posteriors of generators, which is related to the distribution of generated \tilde{y}, \hat{y} and \tilde{x}, \hat{x} . The maximize process can be converted to minimize $C(G)$ without regard to the minus and minimize L1 term $\|\hat{y} - y\|$ and $\|\hat{x} - x\|$ simultaneously. The following lemma shows the conditions of global optimality.

Lemma 2. *The global minimum of the training criterion $C(G)$ can be achieved if and only if $p_y(y) = p_{\tilde{y}}(y) = p_{\hat{y}}(y)$ and $p_x(x) = p_{\tilde{x}}(x) = p_{\hat{x}}(x)$.*

Proof.

$$\begin{aligned} C(G) &= (1 + \gamma) \cdot \mathbb{E}_{y \sim p_y(y)} [(D_A^*(y) - 1)^2] + \mathbb{E}_{y \sim p_{\tilde{y}}(y)} [(D_A^*(y))^2] + \gamma \cdot \mathbb{E}_{y \sim p_{\hat{y}}(y)} [(D_A^*(y))^2] \\ &\quad + (1 + \gamma) \cdot \mathbb{E}_{x \sim p_x(x)} [(D_A^*(x) - 1)^2] + \mathbb{E}_{x \sim p_{\tilde{x}}(x)} [(D_A^*(x))^2] + \gamma \cdot \mathbb{E}_{x \sim p_{\hat{x}}(x)} [(D_A^*(x))^2] \\ &= \int_y (1 + \gamma)p_y \left(\frac{(1 + \gamma)p_y}{(1 + \gamma)p_y + p_{\tilde{y}} + \gamma p_{\hat{y}}} - 1 \right)^2 + (p_{\tilde{y}} + \gamma p_{\hat{y}}) \left(\frac{(1 + \gamma)p_y}{(1 + \gamma)p_y + p_{\tilde{y}} + \gamma p_{\hat{y}}} \right)^2 dy \\ &\quad + \int_x (1 + \gamma)p_x \left(\frac{(1 + \gamma)p_x}{(1 + \gamma)p_x + p_{\tilde{x}} + \gamma p_{\hat{x}}} - 1 \right)^2 + (p_{\tilde{x}} + \gamma p_{\hat{x}}) \left(\frac{(1 + \gamma)p_x}{(1 + \gamma)p_x + p_{\tilde{x}} + \gamma p_{\hat{x}}} \right)^2 dx \\ &= \int_y \frac{(1 + \gamma)p_y(p_{\tilde{y}} + \gamma p_{\hat{y}})}{(1 + \gamma)p_y + p_{\tilde{y}} + \gamma p_{\hat{y}}} dy + \int_x \frac{(1 + \gamma)p_x(p_{\tilde{x}} + \gamma p_{\hat{x}})}{(1 + \gamma)p_x + p_{\tilde{x}} + \gamma p_{\hat{x}}} dx \end{aligned}$$

When the condition is tenable, L1 term is zero, we can get the minimum value of $C(G)$ as $(1 + \gamma)$. Since $\frac{1}{x+1} - \frac{1}{2}$ is a convex function when $x > 0$ and reach zero when $x = 1$, therefore the above is a valid f -divergence.

$$\begin{aligned} C(G) &= 1 + \gamma + \int_y \left(\frac{1}{1 + \frac{(1+\gamma)p_y}{p_{\tilde{y}} + p_{\hat{y}}}} - \frac{1}{2} \right) \times (1 + \gamma)p_y dy + \int_x \left(\frac{1}{1 + \frac{(1+\gamma)p_x}{p_{\tilde{x}} + p_{\hat{x}}}} - \frac{1}{2} \right) \times (1 + \gamma)p_x dx \\ &= 1 + \gamma + \mathcal{D}_f((1 + \gamma)p_y \| (p_{\tilde{y}} + p_{\hat{y}})) + \mathcal{D}_f((1 + \gamma)p_x \| (p_{\tilde{x}} + p_{\hat{x}})) \end{aligned} \quad (13)$$

According to the property of f -divergence, which is always non-negative. The \mathcal{D}_f can be zero only when that two distribution equal, that is $(1 + \gamma)p_y(y) = p_{\tilde{y}}(y) + \gamma p_{\hat{y}}(y)$ and $(1 + \gamma)p_x(x) = p_{\tilde{x}}(x) + \gamma p_{\hat{x}}(x)$. Then take the L1 term into consideration, if we want that achieve its minimum, there must be $p_{\tilde{y}} = p_y$ and $p_{\tilde{x}} = p_x$, so the global minimum of training criterion $C(G) + L_1$ can be achieved if and only if $p_y(y) = p_{\tilde{y}}(y) = p_{\hat{y}}(y)$ and $p_x(x) = p_{\tilde{x}}(x) = p_{\hat{x}}(x)$. \square

A.4. Boost Semantic Color distribution

We have show Bayesian cyclic model generate realistic landscapes with extensive color distribution. Now we present the comparison of semantic color distribution in the following figure. Since the sampling and regularized priors in Bayesian CycleGAN enhance the sharpening effect of adversarial loss in gradient descend process, which in turn make generated semantic distribution closer to the true data. Bayesian CycleGAN boost sharpening and realistic distribution. The following plot show the marginal distributions over generated semantic color values in Lab color space, demonstrating above claim.

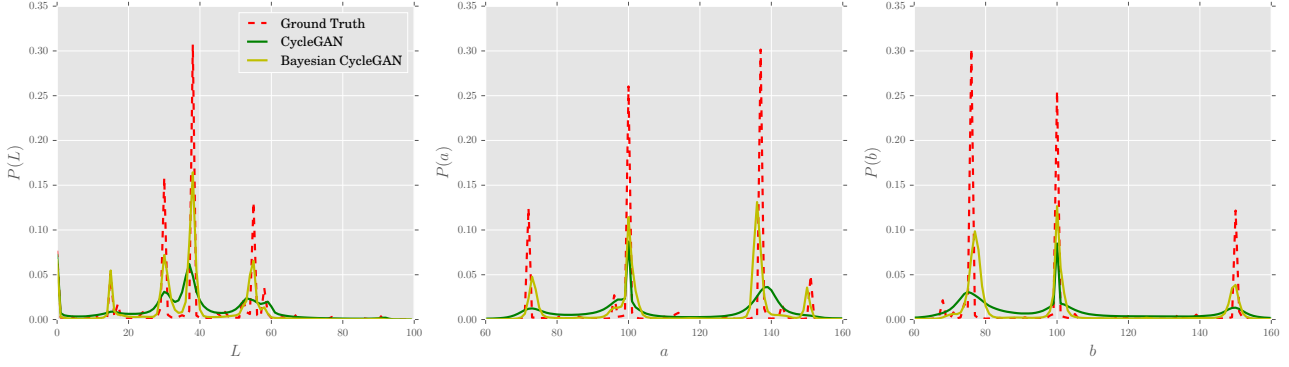


Figure 11. Color distribution matching property of different methods, tested on Cityscapes.

A.5. Algorithm

Algorithm 1 MAP with Monte Carlo latent sampling for training Bayesian CycleGAN. This is one iteration of updating parameters of generators and discriminators.

- Get parameters $\{\theta_{ea}\}, \{\theta_{eb}\}, \{\theta_{ga}\}, \{\theta_{gb}\}, \{\theta_{da}\}$ and $\{\theta_{db}\}$ from previous iteration.
- for** number of mini-batch n in one iteration **do**
 - Extract m_x samples $x^{(1)}, \dots, x^{(m_x)}$ from $p_x(x)$, each x^l has n samples. Use encoder E_A to get SFM $\{f_x^l\}_{l=1}^{m_x}$. Then, combine f_x with batch y^j to get $y_f^{(j)}$.
 - Extract m_y samples $y^{(k)}, \dots, y^{(m_y)}$ from $p_y(y)$, each y^k has n samples. Use encoder E_B to get SFM $\{f_y^k\}_{k=1}^{m_y}$. Then, combine f_y with batch x^i to get $x_f^{(i)}$.
 - Generate \tilde{x} and \tilde{y} by use of G_A and G_B , which take $x_f^{(i)}$ and $y_f^{(j)}$ as input variables. Then combine the fake outputs with SFM $f_x^{m_x}$ and $f_y^{m_y}$ extracted last steps as input to reconstruct cyclic results $\hat{x}^{(i,k)}$ and $\hat{y}^{(j,l)}$ with marginal distribution.
 - Update generators by ascending its posteriors $p(\theta_{ga}, \theta_{gb} | \theta_{da}, \theta_{db})$

$$\nabla_{\theta_g, \theta_e} \left(\frac{\partial \log p(\theta_{ga}, \theta_{gb} | \theta_{da}, \theta_{db})}{\partial \theta_g} + \frac{\partial \lambda_{KL} \mathcal{L}_{KL}}{\partial \theta_e} \right)$$

- Update discriminator by ascending its posteriors $p(\theta_{da} | t, \theta_{ga}, \theta_{gb})$

$$\nabla_{\theta_{da}} \left(\frac{\partial \log p(\theta_{da} | t, \theta_{ga}, \theta_{gb})}{\partial \theta_{da}} \right)$$

- Update discriminator by ascending its posteriors $p(\theta_{db} | t, \theta_{ga}, \theta_{gb})$

$$\nabla_{\theta_{db}} \left(\frac{\partial \log p(\theta_{db} | t, \theta_{ga}, \theta_{gb})}{\partial \theta_{db}} \right)$$

- Append $\theta_{ga}, \theta_{gb}, \theta_{ea}, \theta_{eb}, \theta_{da}, \theta_{db}$ to dataset.

end for
